28 Mar 2001, 4:00 pm - 6:30 pm

A Case History on Soil and Topographic Effects in the 7th September 1999 Athens Earthquake

P. V. Kallou
National Technical University of Athens, Greece

G. Gazetas
National Technical University of Athens, Greece

P. N. Psarropoulos
National Technical University of Athens, Greece

A CASE HISTORY ON SOIL AND TOPOGRAPHIC EFFECTS IN THE 7th SEPTEMBER 1999 ATHENS EARTHQUAKE

P. V. Kallou
National Technical University, Athens, Greece

G. Gazetas
National Technical University, Athens, Greece

P. N. Psarropoulos
National Technical University, Athens, Greece

ABSTRACT

Large concentration of heavy damage to residential and industrial buildings occurred in the small community of Adámes, near the banks of the Kifisos river canyon, during the 7-September-1999 Earthquake. To explore whether the particular topographic relief and/or the actual soil profile have contributed to the observed concentration and non-uniform distribution of damage within a 300 m zone from the edge of the canyon cliff, wave propagation analyses are conducted in one and two dimensions. Soil layering and stiffnesses are determined from 10 SPT-boreholes and 4 crosshole tests. Ricker wavelets and six realistic accelerograms are used as excitation. The results show that the 2D topography effects are substantial only within 50 meters from the canyon ridge, but these effects materialize only in the presence of the relatively soft soil layers that exist in the profile at a shallow depth. The so-called *Topographic Aggravation Factor* (defined as the 2-D / 1-D Fourier spectral ratio) varies from 1.5 to 2.0 over a broad frequency band which covers the significant excitation frequencies. At the location of four collapsed buildings, about 250 m from the edge, 2D (topography) effects are negligible, but the specific soil profiles amplify one-dimensionally all six ground base excitations to spectral acceleration levels that correlate well with the observed intensity of damage.

INTRODUCTORY SUMMARY: EARTHQUAKE and DAMAGE

The M_s 5.9 earthquake ruptured an unmapped blind normal fault. While the exact location of the epicenter and the extent of the rupture zone of the event are still being debated among seismologists, **Fig. 1** portrays three possible candidates for the surface projection of the fault plane. Detailed seismological information can be found in Papadopoulos et al (2000), Stavrakakis (1999), Delibasis et al (2000), Voulgaris et al (2000), Papadimitriou et al (2000), Rondogianni et al (2000).

The fault-plane solutions of the mainshock and the spatial distribution of aftershocks seem to suggest that: (a) the fault plane is dipping at an angle of about 55° to SSW direction, but becomes more vertical at its eastern end; (b) the rupture originated at a depth of about 8-15 km and propagated upwards, with the number of aftershocks being greater in the eastern part of the fault, i.e. the part closer to Athens. One would therefore expect *forward–directivity* effects to have been present in the ground motions experienced at sites located to the east of the rupture zone, at distances within a few kilometers; (c) it appears that the rupturing process stopped under the Aegaleo Mountain range, whose orientation is nearly perpendicular to the strike of the activated fault; the mountain seems to have acted as a barrier, forcing the rupturing process to turn north and thereby activate other faults. The sudden stopping/turning of the rupturing process would have the effect of an impact, generating high acceleration high–frequency waves.

The structural damage was extensive in the NNW part of the Athens metropolitan region: about 100 residential and industrial buildings collapsed, and more than 1500 buildings were damaged "beyond repair". *Repairable* damage was far more widespread over a metropolitan region with about 1.5 million inhabitants. More significantly, 143 people died under the ruins of 29 buildings; their location is depicted in **Figs 1 and 2.** This constitutes one of the largest casualty figures for an earthquake in Greece during this century.

The geographical distribution of buildings the collapse of which caused fatalities is indicative of the intensity of

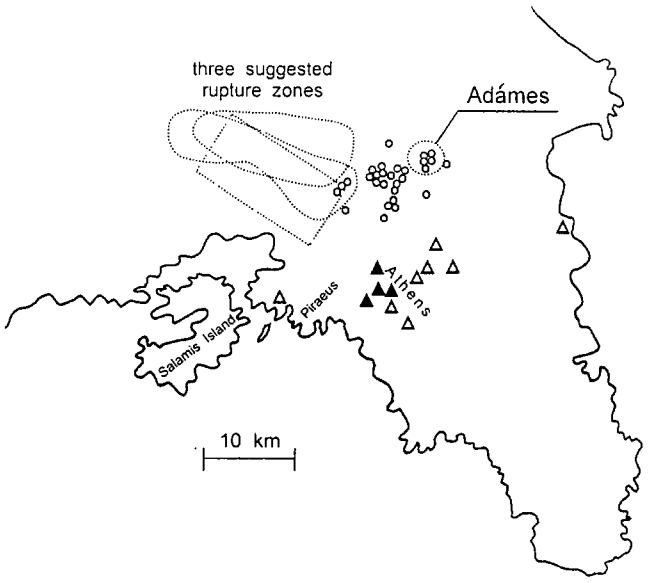

Figure 1
Sketch of the map of the earthquake stricken region showing three possible surface projections of the fault, as proposed in the seismological literature. Most of the accelerograph stations (triangles) were close to the city-center; four of them (shown with filled triangles) are utilized in our study. The severely damaged regions (including the studied area of Adames) were 10-15 km to the north of the city center. The circles show the location of the 28 collapsed buildings with human casualties.

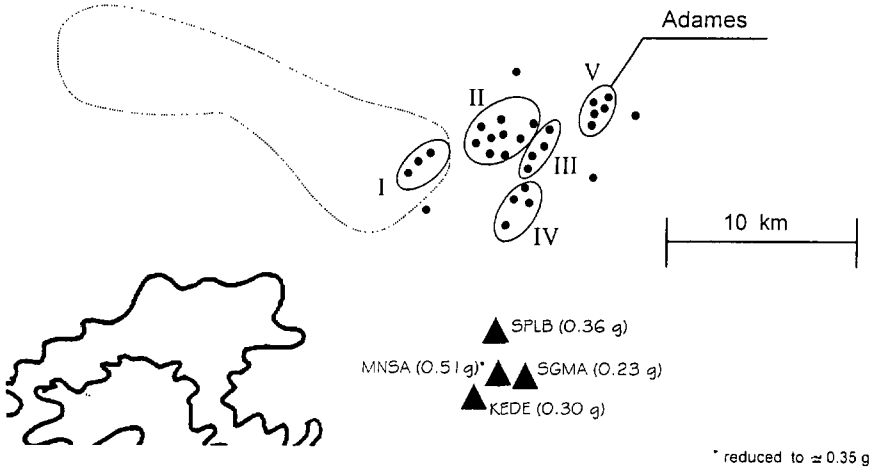

Figure 2
Enlarged map showing the regions of collapsed buildings (I to V) and the four largest recorded values of PGA

damage in the various towns and regions. Five regions are distinguished in **Fig. 2** with their characteristics listed in **Table 1**.

egion No	Name	Observed MMI Max	Min	Distance to fault* (km)
I	Ano Liosia	IX	VIII	1 – 3
II	Menidi	IX	VII +	3 – 5
III	Chelidonoú	IX	VII +	6 – 7
IV	Metamórphosis	VIII+	VII -	7 – 8
V	Adámes	IX	VIII -	8 – 10
	Kamateró	VIII	VII +	5 – 6
	Petroúpolis	VIII -	VII	7 – 8
	Peristeri	VII +	VII	8 – 10

** The range in distance reflects not only the size (in area) of each town/region but also the different seismological views on the ruptured fault and its projection to the ground surface.*

Table 1 : Damage Intensity in regions / towns of collapsed buildings (I – V) compared to damage in three nearby towns

The region called Adámes is a community of medium to low population density, roughly 1200 m in length and 300 m in width, lying next to the deepest canyon of Kifisos river, the main river of the Athens metropolitan area. Built mostly in the 1970's and early 1980's, and administered by the neighboring affluent suburb of Kifisia, Adámes comprises mainly 2-storey to 4-storey reinforced concrete buildings, with very few 1-storey houses and 5-storey buildings.

Overall, structural quality in Adámes is judged as being ***not worse*** (or even perhaps better)than that of the buildings in numerous other towns located between the center of Athens and the earthquake source (such as Kamatero, Petroupolis, Peristeri), at equal or smaller distances from the source. Yet, the MMI in these four towns/regions did not exceed VIII (compared to Adámes : IX), while there were only two casualties in a single collapsed building. (The total population of these towns is nearly half a million). By contrast, in Adámes (total population of about 3,000) the collapse of three industrial and two residential buildings caused 18 deaths, in addition to several safe extrications. Many other buildings either collapsed or had their ground floor (usually a "soft", columns–only, storey) destroyed, and were subsequently demolished. Their location is depicted in **Fig. 3.** The number of floors ranged mostly from 2-4, and the year of construction from 1970 to 1985 with few exceptions.

In the map of **Fig. 3** it is clear that damage is greater in at least two regions : one right next to the Kifisos canyon (within one or two blocks from the crest of the cliff) --- Site 3, and one at a distance of about 200 to 300 meters from it --- Site 2. Some scattered (but less spectacular) damage is also observed at intermediate distances.

A topographic survey of the canyon (by the Survey Division of the National Technical University of Athens, March-April 2000) produced the two sections (M-M' & K-K') shown in **Fig. 4** (see also **Fig. 3**). The slightly idealized geometry used in our investigation is also shown in this figure. Notice the 40 m depth and the nearly 2:1(= h:v) slope of the cliff of the canyon.

The geotechnical investigation of the area comprised the drilling of ten (10) boreholes with SPT measurements and laboratory testing. Eight of these were performed down to a depth of about 35 m, and two reached almost 80 m. Some indirect evidence for greater depths was "extrapolated" from two 150-m-deep boreholes drilled for the under-construction Olympic Village, 1.5 km west to northwest of Adámes. In addition, shear-wave-velocity profiles were obtained at four locations with use of the crosshole technique.

The overall picture emerging from this investigation is re-capitulated in **Figure 5**, in which typical N_{SPT} and low-strain V_S profiles are constructed for Sites 1, 2, and 3 (their location is shown in **Fig. 3**). The following conclusions are drawn :

- All profiles comprise alternating soil layers of silty-gravely sands and sandy-gravely clays to a depth of 20 - 30 m from the surface. In some boreholes intervening layers of sandstone or marl were also found.
- There is a broad qualitative agreement between corresponding N_{SPT} and V_s profiles, although the presence of limestone fragments in some layers leads to spuriously high values of N_{SPT} for a quantitative correlation.
- The approximate average velocity, $\overline{V}_S$, of the soil layers for the three sites is given in **Table 2:**

Site	$\overline{V}_S$ (m/s)	Thickness (m)
1	500	30
2	400	30
3	340	30

Table 2 : Approximate average values of shear–wave velocity at three sites in Adámes

They are indicative of very stiff (Site 1), just stiff (Site 2), and moderately stiff (Site 3) soil profiles. Note that, according to the 1997 NEHRP Provisions (e.g. Dobry et al 2000), the sites would be

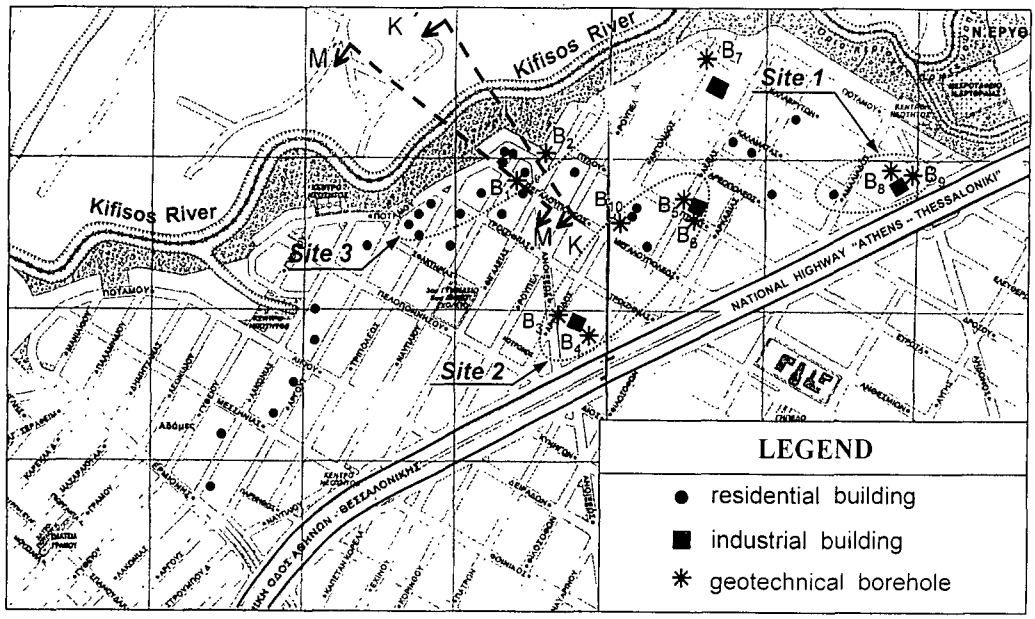

Figure 3
Plan view of Adames showing the heavily damaged and collapsed residential and industrial buildings. The location of the geotechnical boreholes (B_1 - B_{10}) and of the two topographic cross sections (K-K′ & M-M′) are also presented.

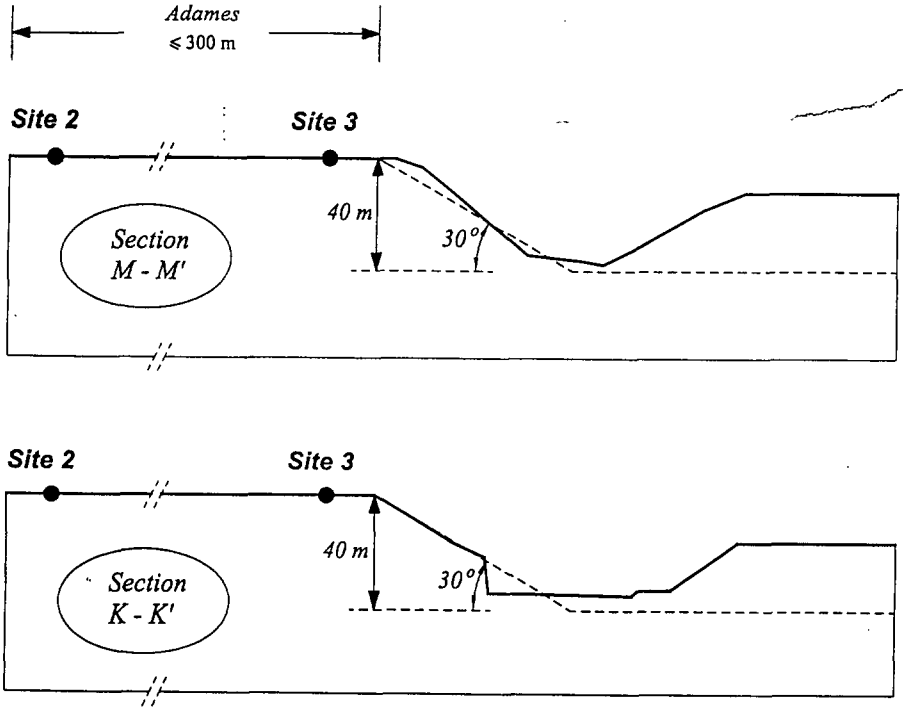

Figure 4

Typical cross sections of the topographic relief of Kifisos River canyon and the region of Adames. Site 3 is located 10 to 50 meters from the edge of the cliff, while Site 2 at about 250 m. The idealized geometry used in our 2-D analyses is also shown (dashed line).

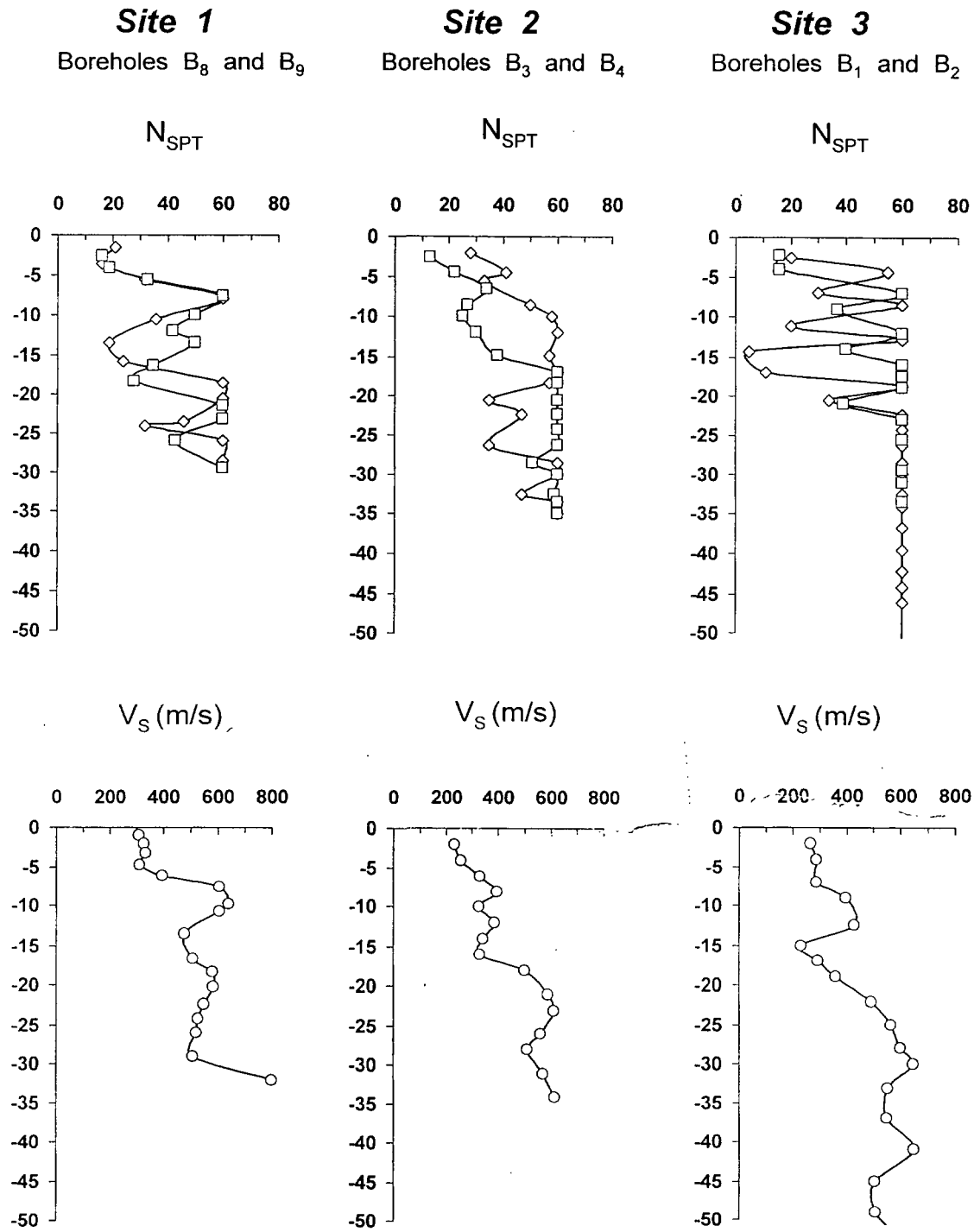

Figure 5
Standard Penetration Test values, N_{SPT} , and crosshole shear wave velocity, V_S , measured near Site 1 , Site 2 ($x \approx 250$ m), and Site 3 ($x \approx 10$ - 50 m). The location of boreholes B_1, B_2, B_3, B_4, B_8, and B_9 are given in Fig. 3(a).

categorized as category C (very stiff soil : 360 < $\overline{V}_S$ (m/s) < 760, $\overline{N}_{SPT}$ > 50),and category D (stiff soil : 180 < $\overline{V}_S$ (m/s) < 360, $\overline{N}_{SPT}$ > 15).

- Although no bedrock was found down to a depth of 80 m, the layers beneath 30 m depth include soft rocks (marls and sandstones) with $V_s \approx 550 - 800$ m/s.

THE STRONG-MOTION RECORDS OF THE EARTHQUAKE

Fifteen strong-motion accelerograph stations were triggered by the main shock within 25 km from the causative fault. They recorded peak ground accelerations (PGA) ranging from about 0.05 g up to 0.50 g. Unfortunately however, there were no records in the meizoseismal area. **Fig. 1** shows the location of the accelerograph stations. Emphasis is given on the four stations with the strongest (in terms of PGA) motions (shown as filled triangles in the figure): the station name, its largest PGA, and its approximate distance from the earthquake source are given in **Table 3** :

Station Name (Symbol)	Largest PGA	Distance (km)
MONASTIRAKI (MNSA)	0.51 g	10
SEPOLIA B (SPLB)	0.36 g	8
KEDE (KEDE)	0.30 g	12
SYNTAGMA A (SGMA)	0.23 g	11

Table 3 : Accelerograph stations which recorded the strongest motions (in stations of the Geodynamic Institute and of ITSAK)

We will first briefly examine these recorded motions, to see how much they were affected by the underlying soil and by the presence of adjacent underground structures.

MONASTIRAKI Record

The accelerograph station MONASTIRAKI (MNSA) recorded a very high PGA, 0.51 g, in one direction. The accelerogram and its elastic response acceleration spectrum, SA(T), for 5% structural damping, are plotted in **Fig. 6(a)**. The very low dominant periods that are evident in this record (0.08 and 0.15 seconds) could only partly explain the small degree of building damage in the neighborhood of the station in spite of spectral accelerations exceeding 1.50 g. However, having been recorded next to a deep shaft of an under-construction Metro Station, this accelerogram had aroused suspicion that it might have been affected by the underground structure. Indeed, in addition to the shaft, two other underground "structures" were present very close to the instrument: a heavy-walled shallow tunnel of the old metro line (18 m wide and 10 m deep) and a 5-m-deep open archaeological excavation pit lie between the instrument position and the shaft. The soil profile comprises stiff sandy clays and highly weathered rock formations down to at least 60 m depth. The weighted average value of velocity at depths $z \leq 30$ m is about 400 m/s --- category C according to the NEHRP 1997 Provisions (Dobry et al, 2000).

We implemented an *inverse* numerical procedure, using a finite-element model of the system, with the record under investigation being the target surface motion. Equivalent-linear soil properties were assigned to the soil elements and vertical SV wave excitation was assumed.

The details of this investigation are beyond the scope of the present paper; however, the method of analysis is essentially the same as the one described in the sequel in connection with the study of the Adámes topography.

Our study confirmed that the presence of the three underground structures has indeed spuriously enhanced the acceleration amplitudes in one of the horizontal components of the instrument. Wave diffraction at the corners has apparently led to an increase of about 30% in peak ground acceleration compared to what would have been recorded in a truly free field. **Fig. 7** summarizes the results of the investigation. It shows that the motion recorded at accelerograph station (PGA 0.51g) : (i) could be numerically derived from a base (-60 m) motion of PGA ≈ 0.20 g, and (ii) is consistent with free-field ground-surface acceleration amplitudes of PGA ≈ 0.30g. The latter value is in better agreement with the peak values of the neighboring stations (KEDE 0.30g and SYNTAGMA 0.25 g). For a general description of the base motion, the so-called *rock-outcrop* motion has been computed; it is shown in **Fig. 6(b)** along with its response spectrum. (This motion should be distinguished from the base motion shown in Fig. 9.) Evidently, both *soil flexibility* and *underground "obstacles"* have had their imprint (one-dimensionally and two-dimensionally) on the record.

KEDE and SEPOLIA Records

These two accelerograms are essentially (if not strictly) free-field motions, recorded on the surface of stiff soil deposits. The KEDE profile comprises a 10 m soil stratum of average $V_S \approx 320$ m/s – 400 m/s, with the underlying soft rock having similar stiffness with the base in MONASTIRAKI station. The SEPOLIA profile is somewhat softer: 13 m of alluvium with $V_S \approx 300$ m/s, underlain by stiffer "rock".

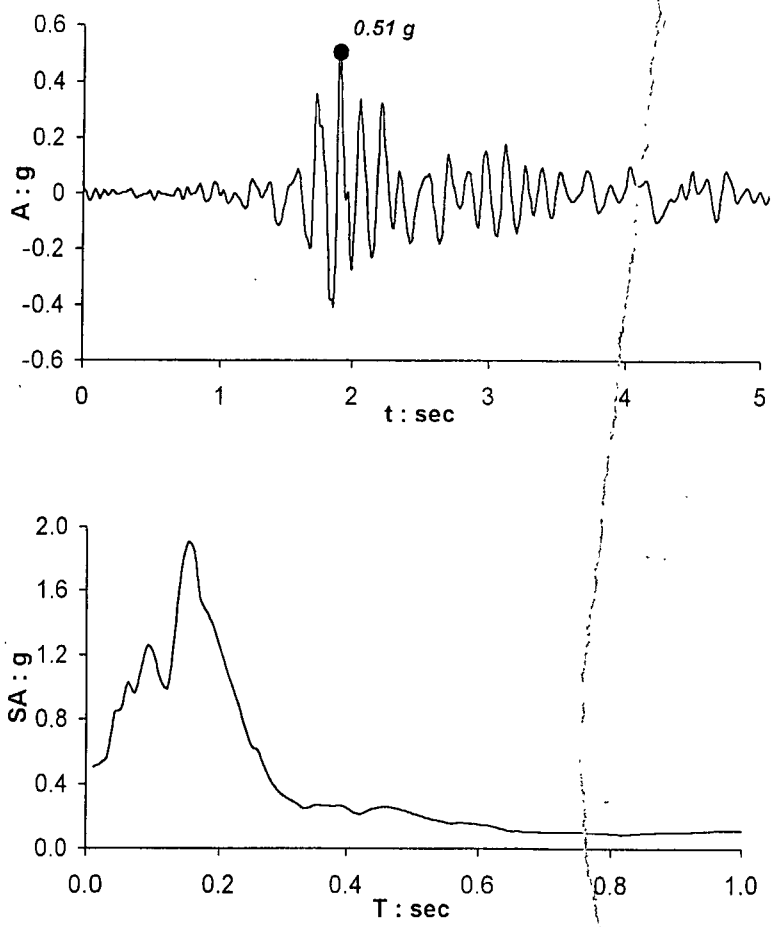

Figure 6(a)

The strongest component of the MONASTIRAKI station (MNSA): accelerogram and 5% damped response spectrum (from Geodynamic Institute N.O.A.)

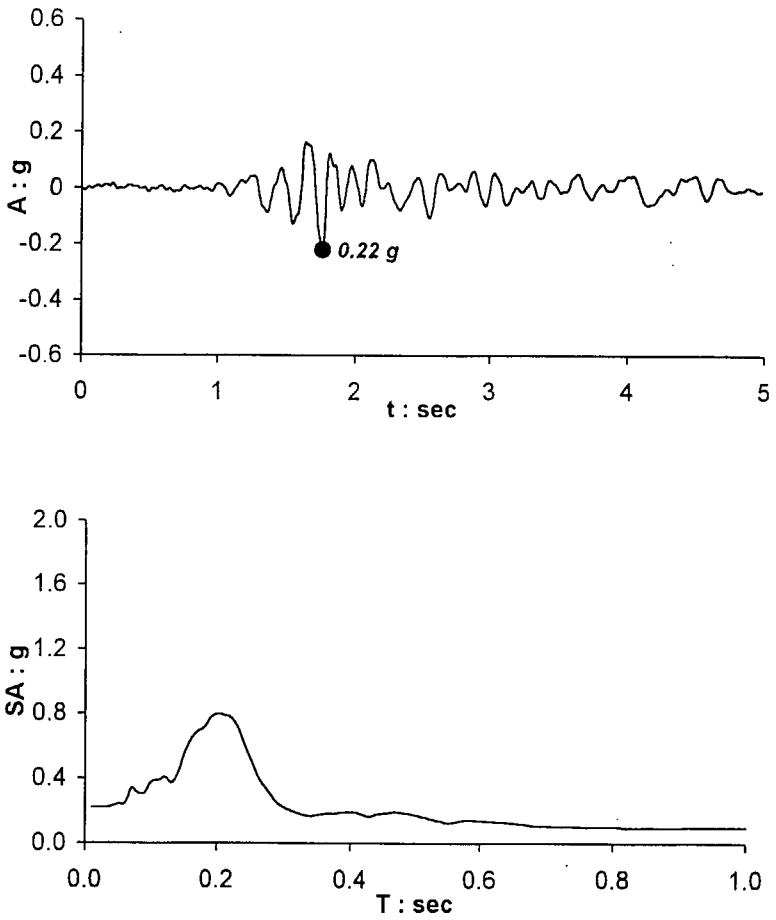

Figure 6(b)

The rock-outcrop base motion deduced from the MONASTIRAKI record

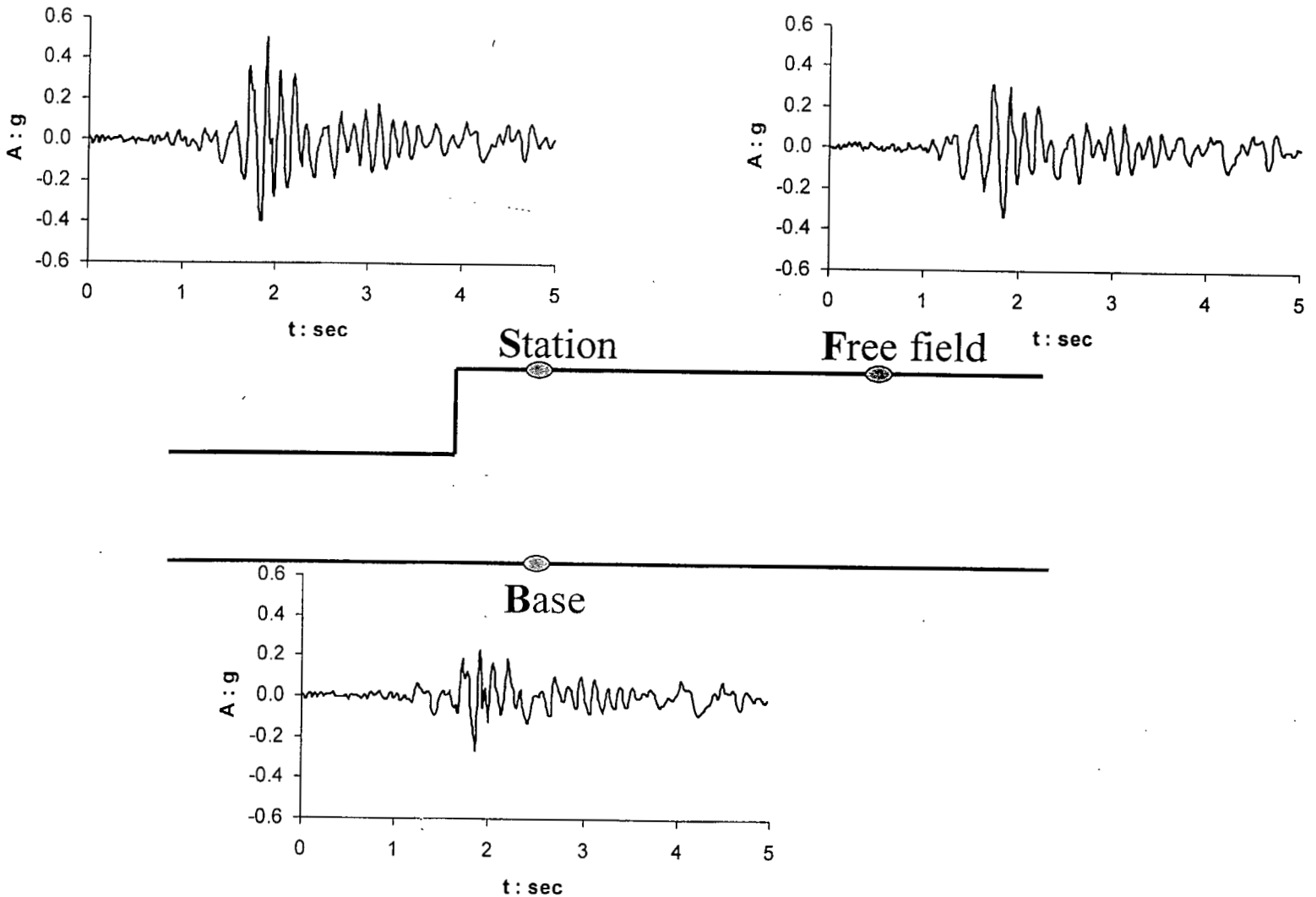

Figure 7

Results of the 2-D deconvolution for Monastiraki, with the free-field surface and base ("within") computed motions

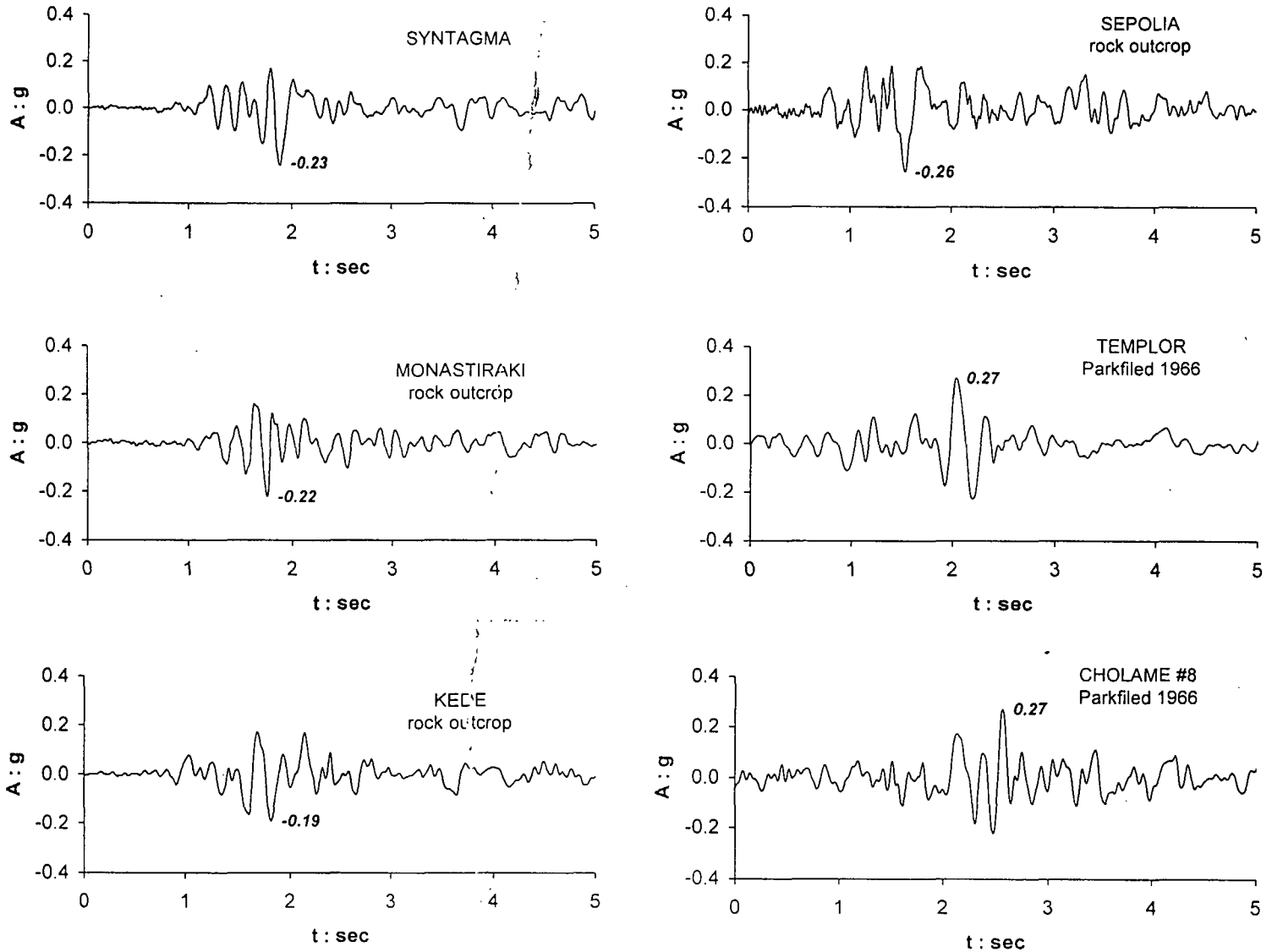

Figure 8(a)

The ensemble of six ground motions computed (on the basis of four actual records) or selected (from the strong-motion world bank) to describe the rock-outcrop motion at a distance of about 10 km from the earthquake source.
(a) acceleration time-histories

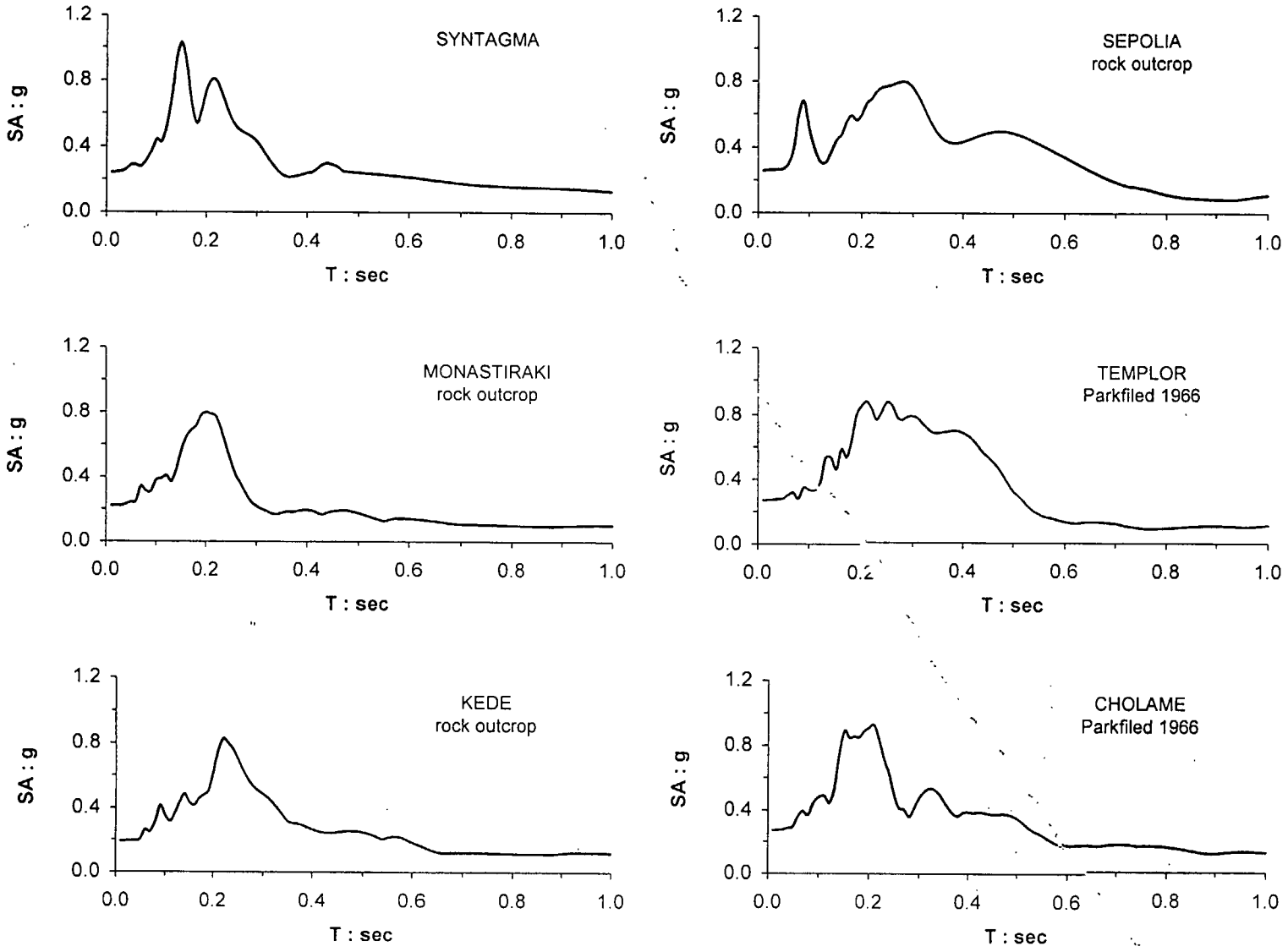

Figure 8(b)

The ensemble of six ground motions computed (on the basis of four actual records) or selected (from the strong-motion world bank) to describe the rock-outcrop motion at a distance of about 10 km from the earthquake source.
(b) acceleration response spectra

One-dimensional equivalent-linear deconvolution analyses have led to the *rock-outcrop* motions given in **Fig. 8**, along with the other motions used as a description of base excitation in this work.

SYNTAGMA Record

This motion (SGMA) was recorded inside a station of the just completed (at that time) Athens Metro, at 7 m depth. There are reasons to believe that the recorded motion was affected by the station structure. However, the ground supporting and surrounding the station is only-slightly-weathered rock, while the spectral characteristics of the recorded motion are rather similar to those of the nearby MONASTIRAKI station. Thereby, we have decided to consider this record as a *rock outcrop* motion, with no modification.

Other Possible Motions

The above four rock-outcrop accelerograms were used as input excitation in Adámes, in view of the roughly similar distances from the surface projection of the fault. To complete an ensemble of six probable base motions, two more (unmodified) accelerograms were selected from the world strong motion data-bank. Both of them are from the 1966 M_S = 5.6 Parkfield, California, earthquake. They were recorded on soft rock at Cholame Shandon No. 8 and Temblor Stations (Leeds, 1992). As seen in **Fig. 8**, these two records (both having a PGA of about 0.27 g) resemble the aforementioned four rock-outcrop motions from the 7-9-99 event, in the time as well as in the frequency domain. Notice that the TEMBLOR response spectrum exhibits a plateau of about 0.70 g in the period range of 0.20 to 0.40 seconds, resembling the SEPOLIA base-outcrop motion.

We believe that the ensemble of these six selected motions offers a realistic and complete description of the free-field base motion for Adámes.

ONE-DIMENSIONAL SOIL AMPLIFICATION STUDIES

To explore the role of the actual soil profiles in modifying the intensity and the frequency characteristics of ground shaking in Adámes, we first perform 1-D equivalent-linear wave-propagation analyses with the code SHAKE (Schnabel et al 1973). The decrease of shear modulus and the increase of material damping with increasing amplitude of shear strain for each soil layer are obtained not from actual laboratory measurements but from established empirical curves (Vucetic & Dobry, 1991). The aforementioned six motions **[Figs. 8(a), (b)]** were used as the input *rock-outcrop* excitation, for each of the three Sites (1, 2, and 3) of **Fig. 3.**

Only a few typical results of analyses are outlined here, with the help of **Fig. 9** (for Site 1), **Fig. 10** (for Site 2), and **Fig. 11** (for Site 3), for the KEDE excitation. Each of the three figures compares the rock-outcrop (base input) and surface (output) acceleration time-histories and the corresponding response spectra; it also portrays the spectra of the ratio of the corresponding Fourier amplitudes ("*Amplification Ratio*"). The following conclusions are drawn :

a) **Site 1** (where the 'Fourlis' industrial building collapsed, killing 8) being the stiffest of the three sites, shows an appreciable degree of amplification. PGA as well as spectral acceleration (SA) values for periods $T = T_a < 0.30$ sec increase by as much as 50% ; at higher periods the SA values for base and surface are merging, becoming essentially the same. The only difference between the results of the various analyses is that for the TEMBLOR and SEPOLIA excitations the period T_a, beyond which soil amplification is insignificant, increases to almost 0.50 seconds. This would be an important difference for three to five story buildings.

b) **Site 2** (where the industrial buildings 'Faran' and 'Prokos', and two residential buildings collapsed) is softer than Site 1. Not surprisingly therefore, that our analyses show a larger amplification over a wider period range. Computed PGA values are in the range of 0.40 g – 0.50 g, and the highest SA reaches 2g at $T \approx 0.22$ seconds. Evidently, there is a pseudo-resonance condition developing at this period : the fundamental period of the soil column ($T_S \approx 0.22$ sec from the Amplification Ratio of **Fig. 10**) nearly coincides with the dominant excitation period ($T_E \approx 0.20$ sec). Recorded aftershock motions in the Faran building (Theodoulidis / ITSAK, and Makropoulos / University of Athens, personal communication) seem to confirm the fundamental period of the 1-D analyses.

c) **Site 3** (next to the canyon, where several buildings collapsed) is the softest of the three sites. The 1-D *Amplification Ratio* spectrum exhibits a broad peak at $T \approx 0.42$ sec, interpreted as the fundamental natural period T_S of the soil deposit. Recall that most of the rock-outcrop excitations have much smaller dominant periods, $T_E \approx 0.10$-0.20 sec. Hence, little or no increase is expected in PGA and in SA values due to soil for $T < 0.25$ sec --- confirmed with the 1-D results of **Fig. 11.** On the other hand, the doubling of Fourier amplitudes computed for the approximate period range of 0.30 - 0.60 sec, could be substantial if the input motion were rich in such relatively-high-period components. This is the case mainly with the SEPOLIA, TEMBLOR, and CHOLAME records.

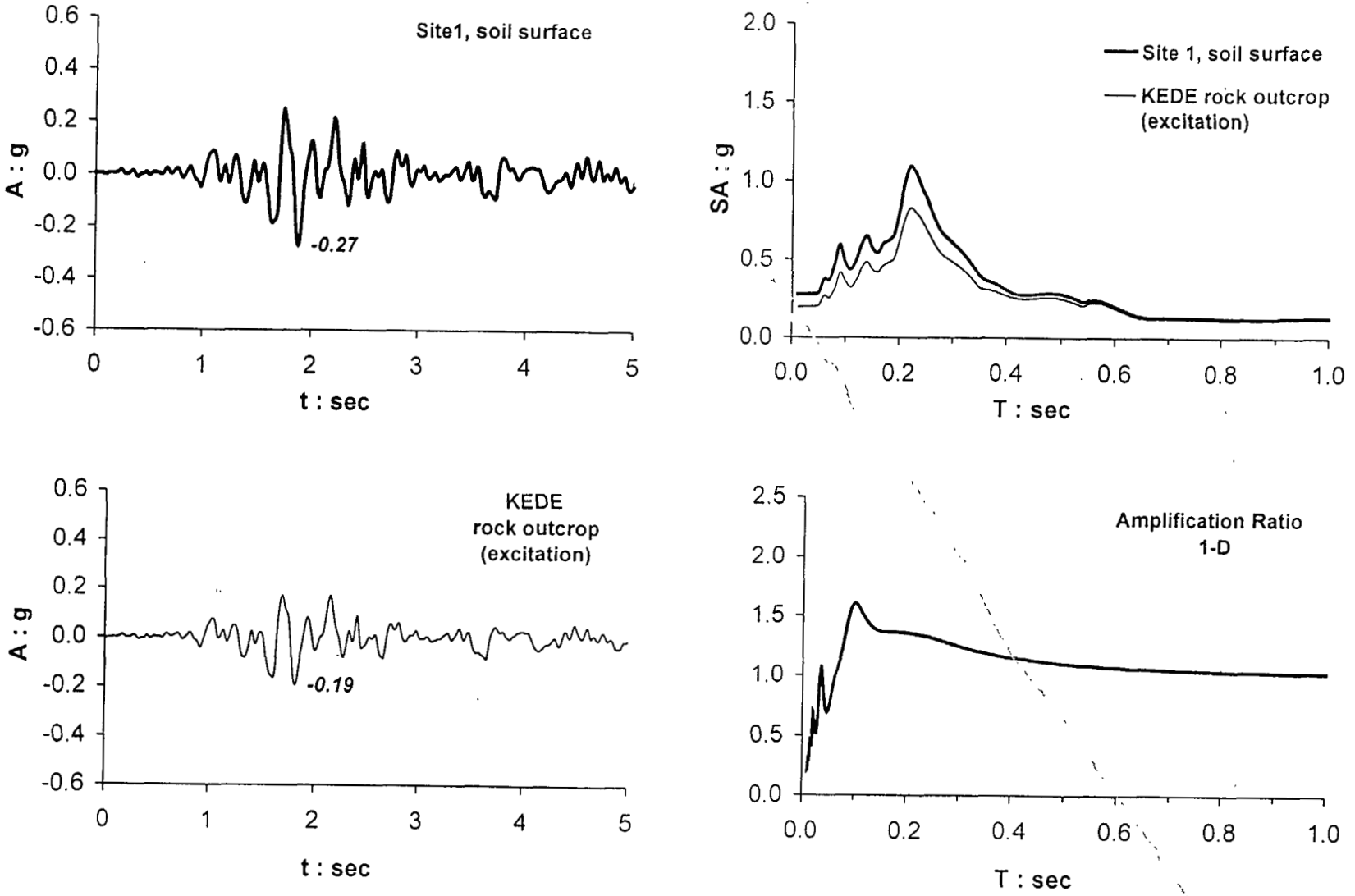

Figure 9

Typical outcome of 1-D soil amplification study for Site 1

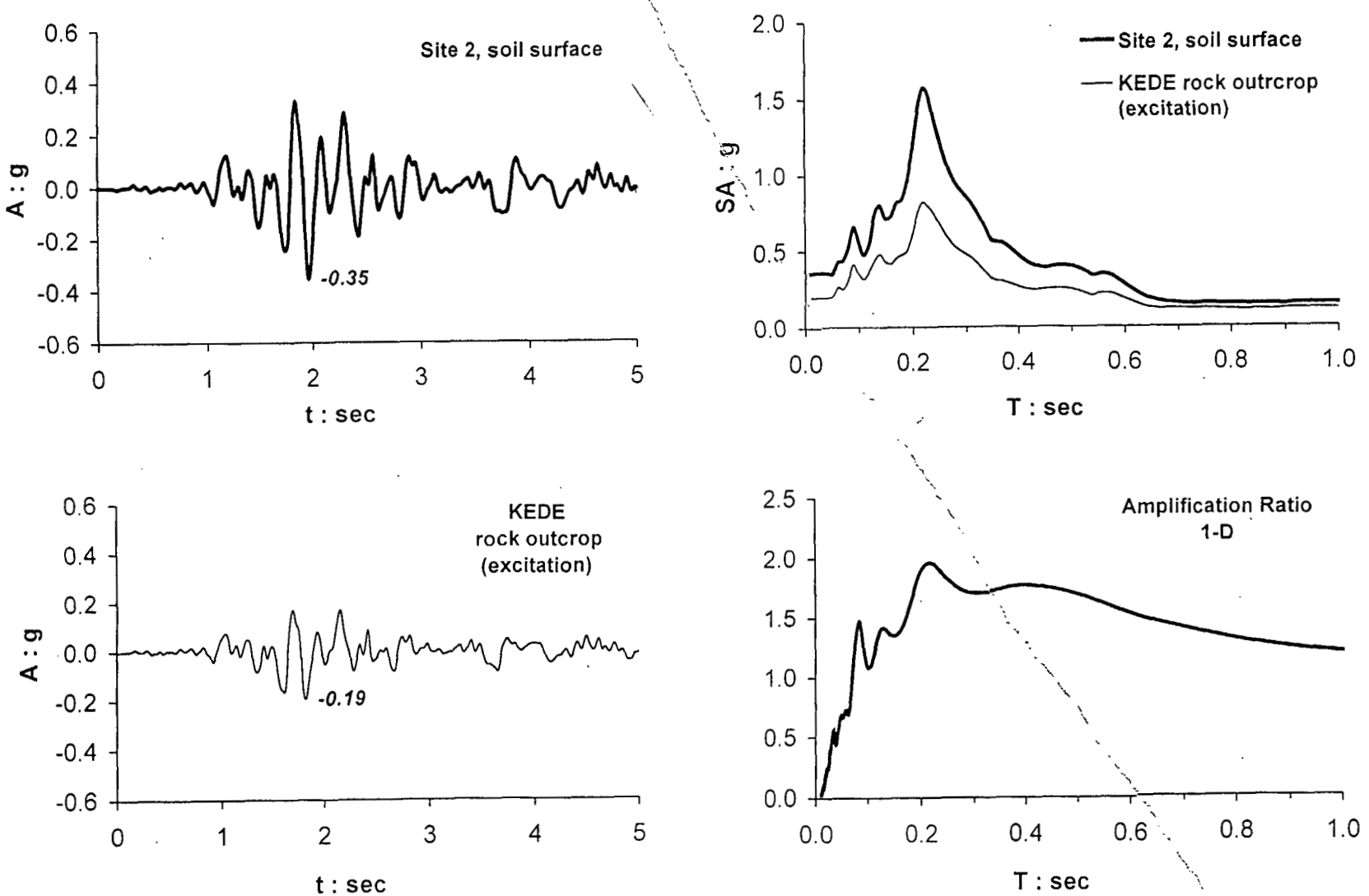

Figure 10

Typical outcome of 1-D soil amplification study for Site 2

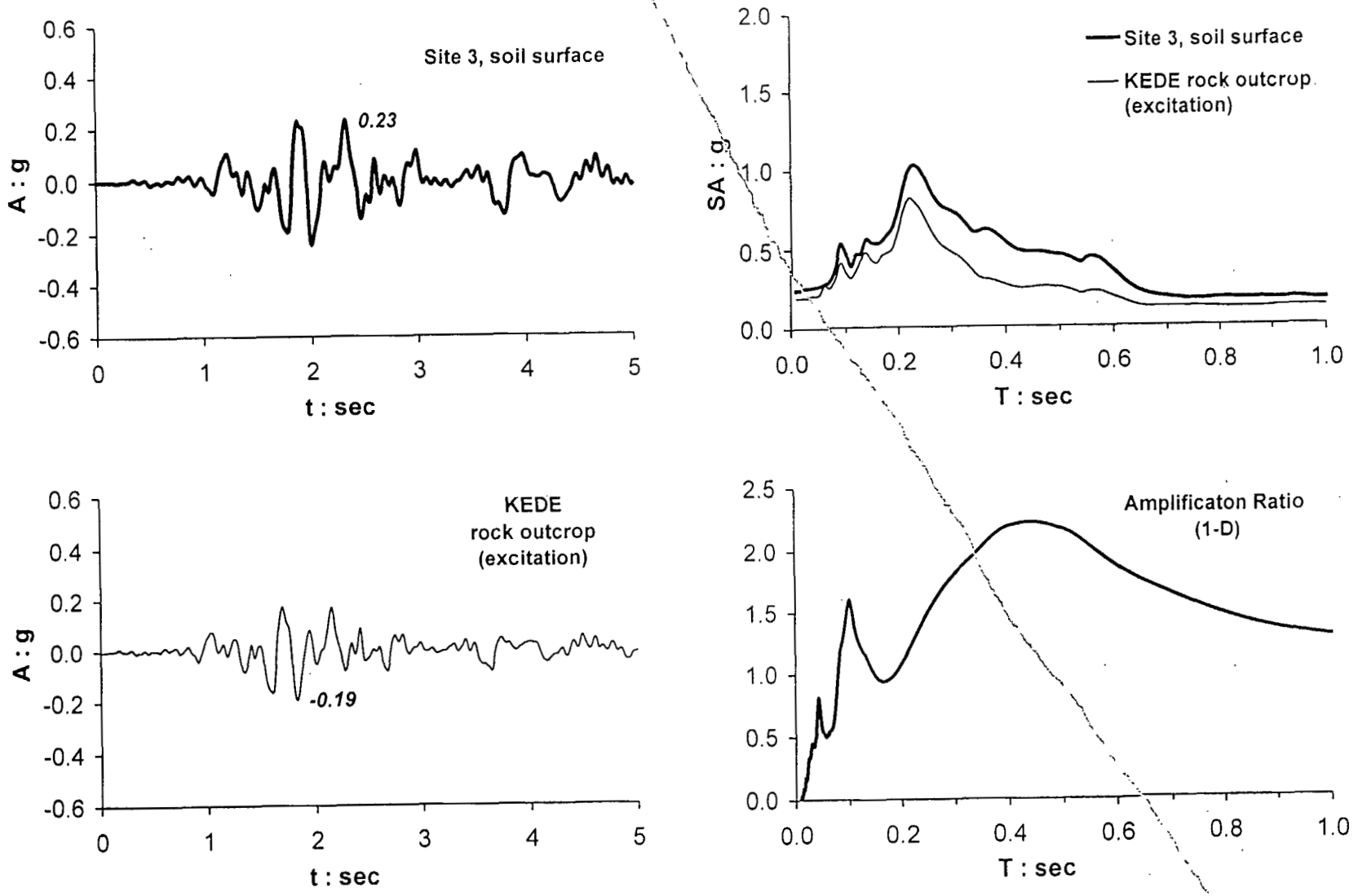

Figure 11

Typical outcome of 1-D soil amplification study for Site 3

Qualitative comparison of the ground surface accelerations (time-histories and spectra) predicted for the three Sites under the assumption of 1-D wave propagation with the observed intensity of damage in Adámes, and with the original recorded motion, leads to the following conclusions:

(a) for Site 2, 1-D soil–amplified motions are stronger than any of the recorded motions, and are compatible with the observed high intensity of damage in that region

(b) for Sites 1 and 3, 1-D soil amplification despite its computed importance would not alone and in all cases suffice to explain the observations – especially in Site 3, one of the most heavily damaged regions in the 7-9-99 earthquake.

It will be shown in the sequel that an additional amplification has been produced by 2-D waves emanating from the cliff of the Kifisos canyon.

TWO-DIMENSIONAL MODELING OF THE CLIFF AND CANYON

The 2-D wave propagation analyses were mostly performed with the finite-element (FE) code ABAQUS (Hibbit et al 1997). The model was based on the soil-properties described in **Fig. 5**. Plane SV waves are assumed, with the six *rock-outcrop* acceleration time histories of **Fig 8(a)** describing the base excitation. Moreover, to develop a deeper understanding on the wave mechanics of the problem, the spectral element code AHNSE (Casadei & Gabellini 1997; Faccioli et al 1997) was also utilized, while the time function of the incident plane–SV wave was taken as a Ricker wavelet of type beta:

$$u(t) = \left[1 - 2b(t - t_0)^2\right]\exp\left[-b(t - t_0)^2\right]$$

where $b = (\pi f_0)^2$, with f_0 the characteristic frequency, and t_0 = time of max$[u(t)]$. The derived acceleration time-histories, ü(t), have been scaled to values compatible with the *rock-outcrop* motions.

The (FE) discretization of the 2-D model is shown in **Fig. 12**. The mesh consists of 8-noded quadrilateral and 6-noded triangular elements, the size of which is kept to less than one-fifth of the smallest significant considered wavelength.

To model realistically the excitation by incident (vertical or inclined) SV waves in ABAQUS, loading is imposed using a special technique, the ***Effective Seismic Excitation*** method, developed by Bielak and his coworkers [Bielak & Christiano (1984), Loukakis (1988) and Bielak et al (1996)]. With this approach the problem of seismic response of a 2-D soil medium is transformed into an equivalent one in which the source is located in the interior of the domain of computation. The advantage of the method is that, as the seismic excitation is introduced directly within the region of interest, the artificial boundary is needed only to absorb the scattered energy of the system. Thereby, viscous dashpots can be placed not only on the lateral boundaries, but at the base of the model as well. In addition, these boundaries may be placed as close to the examined region as the accuracy of the absorbing boundary permits. This option permits the discretization of a limited area of the underlying rock, thereby reducing the computational effort.

Material damping in ABAQUS is of the Rayleigh type, which means that damping is frequency dependent. In addition, soil behavior is hysteretic, represented approximately with an iterative equivalent linear method. The effective material damping in the most heavily –strained upper soil layers was of the order of 7% (corresponding quality factor : Q = 7)

The spectral–element (SE) discretization for the code AHNSE consisted of macro-elements, each subdivided into 16 micro-elements. Element size has been tailored to wavelength. Excitation in AHNSE consisted solely of incident-SV Ricker wavelets. Absorbing boundaries were placed around the domain of interest. Compatible results between FE and SE methods were our prerequisite before embarking in a further detailed investigation.

EFFECT OF TOPOGRAPHY AND SOIL: TWO-DIMENSIONAL RESULTS

The seismic effects of *unusual* topography (meaning: non-plane ground surface, as in the case of canyons, hills, ridges, and cliffs) have been repeatedly shown to be detrimental to structures. Concentration of heavy damage near the crest of cliffs and ridges, or near the top of hills and canyons, has been observed in numerous earthquakes: in Miyagiken-oki 1978, Chile 1985, Southern Germany 1978, Whittier Narrows 1987, Irpinia 1980, and Eje Cafetero–Colombia 1999. (See details in Ohtsuki & Harumi 1983, Celebi 1988, Kawase & Aki 1990, Siro 1982, Restrepo & Cowan 2000).

Instrumental evidence of *topographic amplification* is also abundant in weak seismic environments, but rather limited from strong and destructive seismic shaking. Among the few examples: the Pacoima Dam Abutment record of the 1971 San Fernando Earthquake, two records in the Nahanni 1985 earthquake, and the astonishing records in Tarzana Hill Nursery during the Whittier Narrows 1987 and Northridge 1994 earthquakes (Boore 1973, Leeds 1992, Sanchez-Sesma 1985, Aki 1988, Shakal et al 1988, Bouchon & Barker 1996).

A large number of analytical and numerical studies have provided supporting evidence of the significance of *topographic* effects; methods of analysis and review summaries can be found in: Wong & Trifunac (1974),Bard (1982,1995),Bard & Tucker (1985), Aki (1988), Sanchez-Sesma & Campillo (1991), Sanchez-Sesma (1991), Faccioli (1991), Finn (1991). However, as shown by Geli et al (1988), the simultaneous effect of heterogeneities in subsurface (soil and rock) shear wave velocities may also be significant, although this is not so well documented.(See also Paolucci et al 1999.)

The Adámes case history analysed herein offers such documented evidence of combined topography and soil heterogeneity effects. The results of our parametric investigation are summarized in **Figures 13 - 21**. Specifically:

Fig. 13 refers to the fundamental case of a homogeneous halfspace with a canyon subjected to Ricker type excitation (f_o = 3 Hz). It portrays the distribution along the ground surface of the normalized peak horizontal, A_H, and vertical, A_V, accelerations. Damping in the halfspace is maintained at the level of 5% (average value of the equivalent linear 1-D analyses), while V_S is taken as 550 m/s, typical of the stiff clays and marls encountered in the earthquake-stricken region. It is seen that the topographic effect is noticable but not substantial for *vertically* incident SV waves : horizontal accelerations, A_H , increase by a factor of almost 1.2 within 50 m from the edge of the cliff, compared to the free-field value, while a vertical component $A_V \approx 0.20A_H$ develops collaterally. Admittedly however, this effect is frequency-dependent; the broad-band nature of the Ricker wavelet does not emphasize the potential importance of certain frequencies.

Fig. 14 illustrates that in a layered medium corresponding to the profile of Site 2 the crest amplification rises to 1.35 for the horizontal acceleration, but then diminishes very rapidly away from the edge. The collateral vertical component, A_V, equals almost 0.20 A_H. It is recalled that equivalent linear properties were assigned to each soil layer, with damping values ranging from 4% to 7% in the upper 30 m. It is noted that the above values of topographic amplification are qualitatively and quantitatively similar to those reported for a steep cliff (slope h : v = 1 : 2) by Ohtsuki & Harumi (1983), for incident harmonic SV wavelengths λ = 2H and λ = 4H. In our case, for the central Ricker frequencies $f \approx f_o$ to $3f_o$, with f_o being the characteristic frequency, the dominant wavelengths are in the range $\lambda \approx$ 1H to 5H, which encompasses the range of Ohtsuki & Harumi: hence the validity of our successful crude comparison. It is also worth recalling the finding of Wong & Jennings (1975), that the effect of (a cylindrical canyon) topography is strongest under harmonic steady-state excitation for wavelengths λ comparable to canyon width B (which equals 2H). Time-domain solutions do not show as large a topographic amplification, while acceleration response spectra show the smallest amplification, and only at high frequencies (Aki 1988). Hence, to ensure that our conclusions would not be biased in exaggerating the topography effects, we present sufficient time-domain results and compare mostly acceleration response spectra.

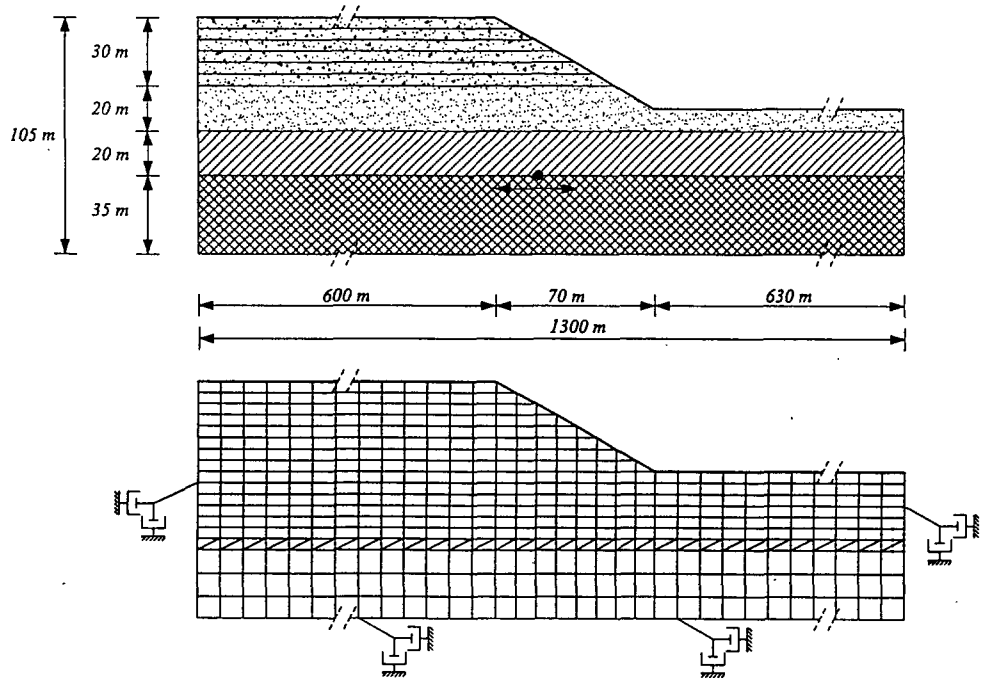

Figure 12

The 2-D finite-element model of the cliff and the soil

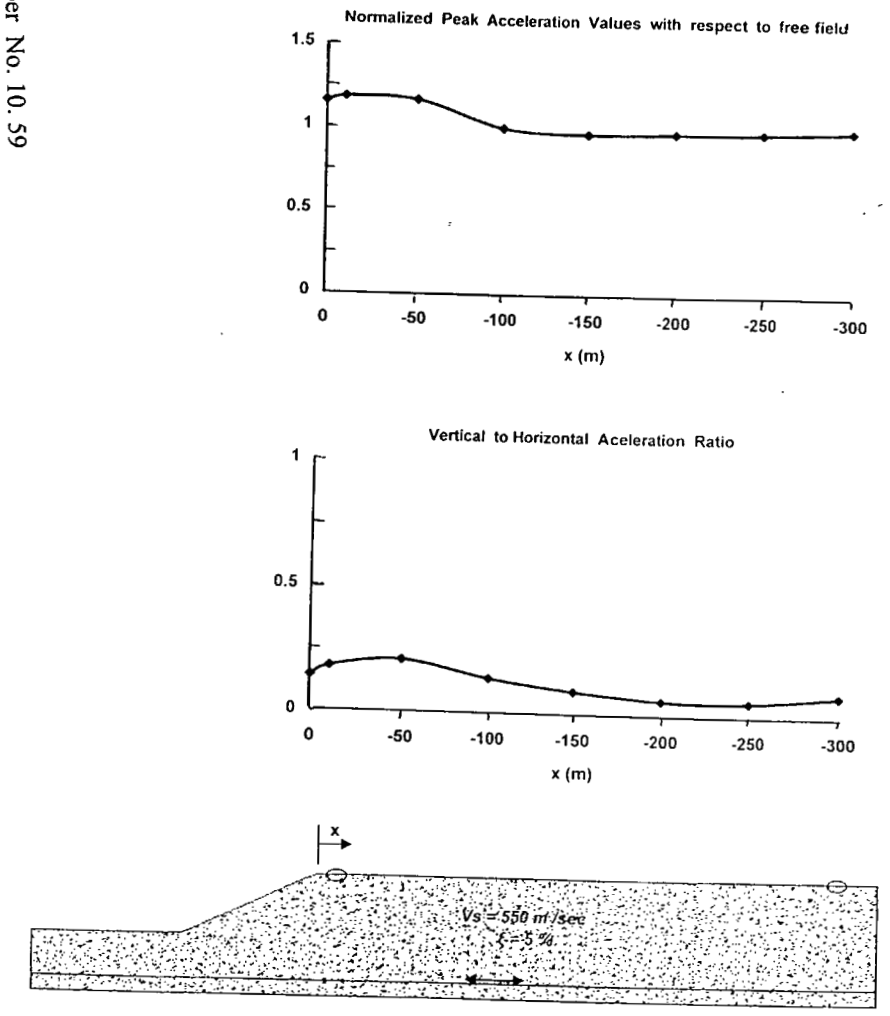

Figure 13

Adámes cliff consisting of a homogeneous halfspace: distribution of normalized horizontal and vertical peak surface accelerations with a Ricker $f_o = 3$ Hz wavelet as vertical SV-wave excitation

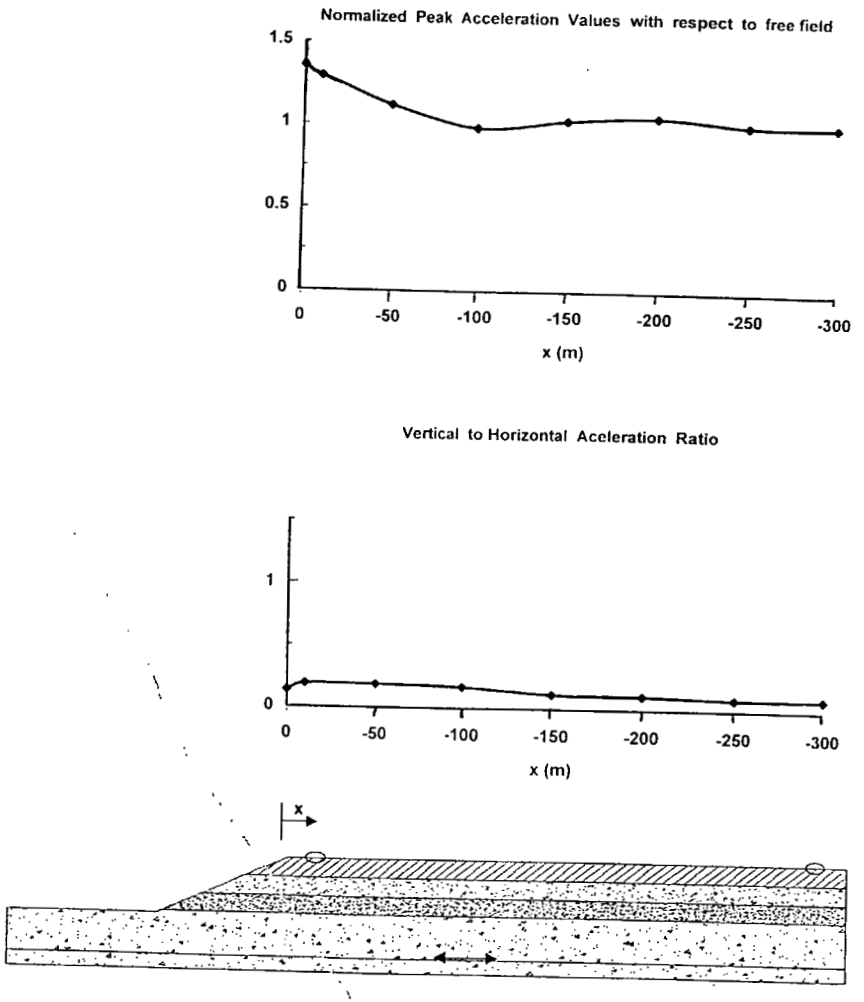

Figure 14

Adámes cliff consisting of a layered medium (profile of Site 2): distribution of normalized horizontal and vertical peak surface accelerations with a Ricker $f_o = 3$ Hz wavelet as vertical SV-wave excitation

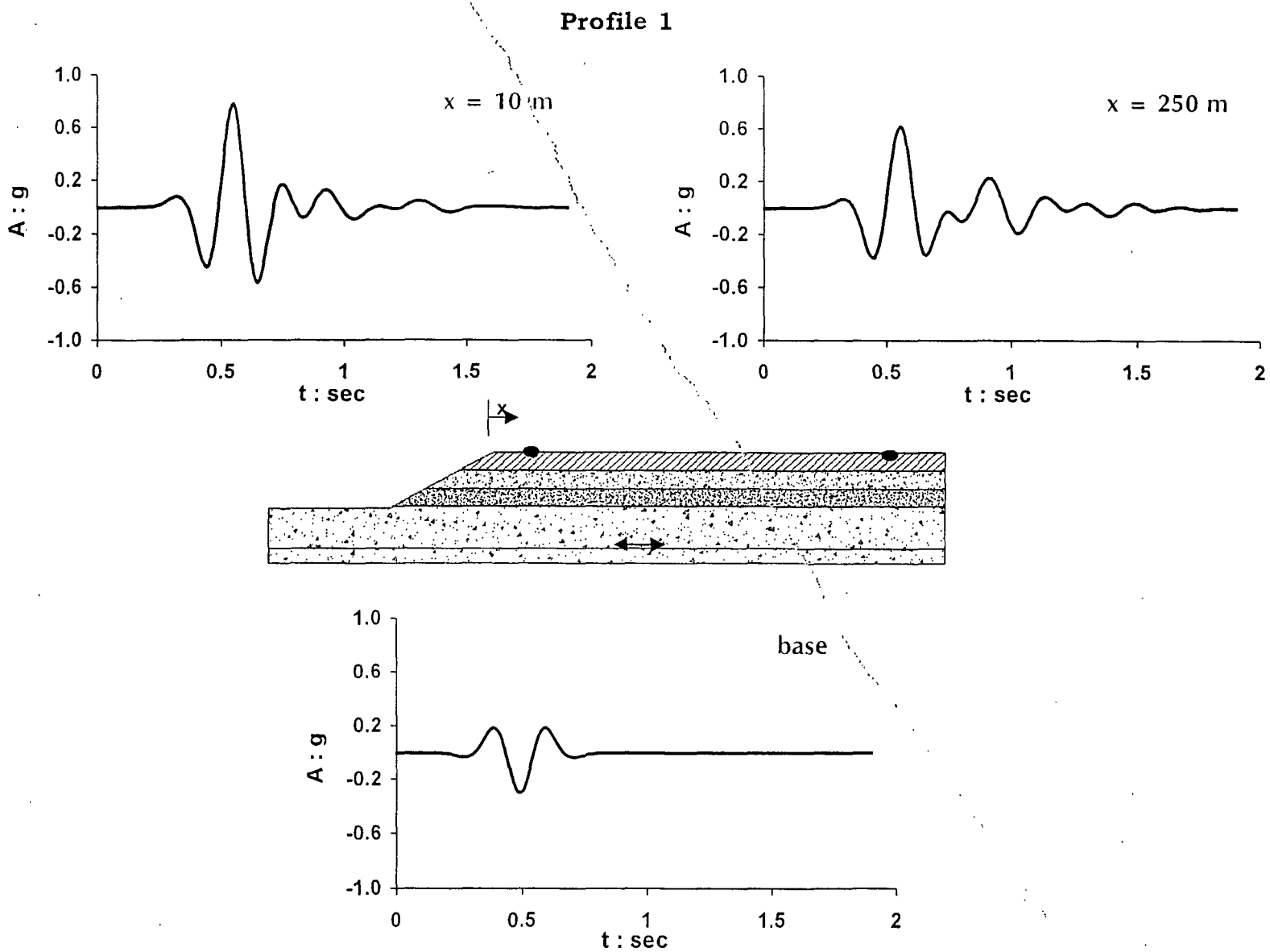

Figure 15

Adámes cliff with a layered halfspace (soil profile of Site 1): computed time histories of horizontal acceleration at x = 10 m (Site 3) and x = 250 m (Site 2). Ricker f_o = 3 Hz wavelet as vertical SV-wave excitation

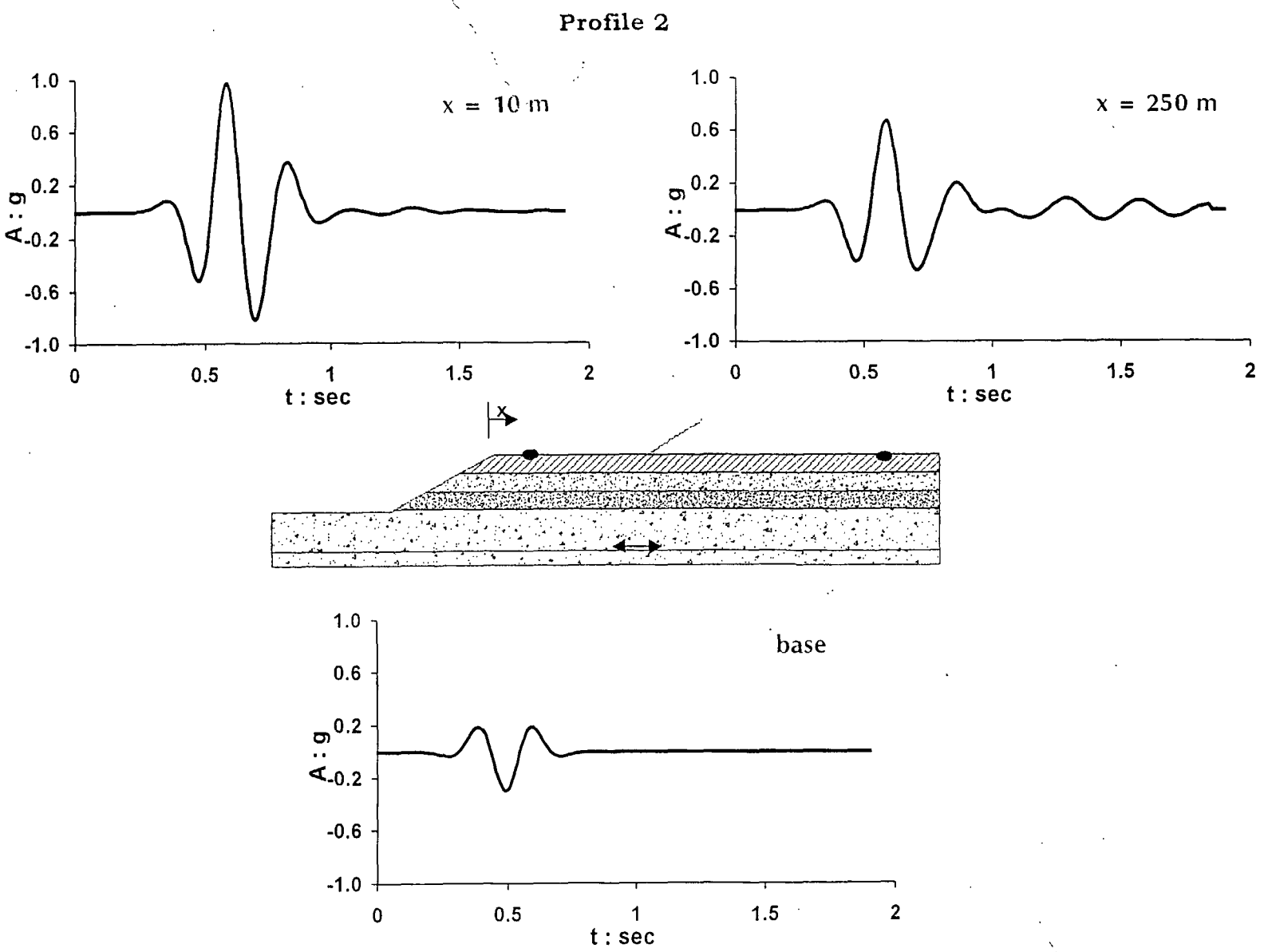

Figure 16

Adámes cliff with a layered halfspace (soil profile of Site 2): computed time histories of horizontal acceleration at x = 10 m (Site 3) and x = 250 m (Site 2). Ricker f_o = 3 Hz wavelet as vertical SV-wave excitation

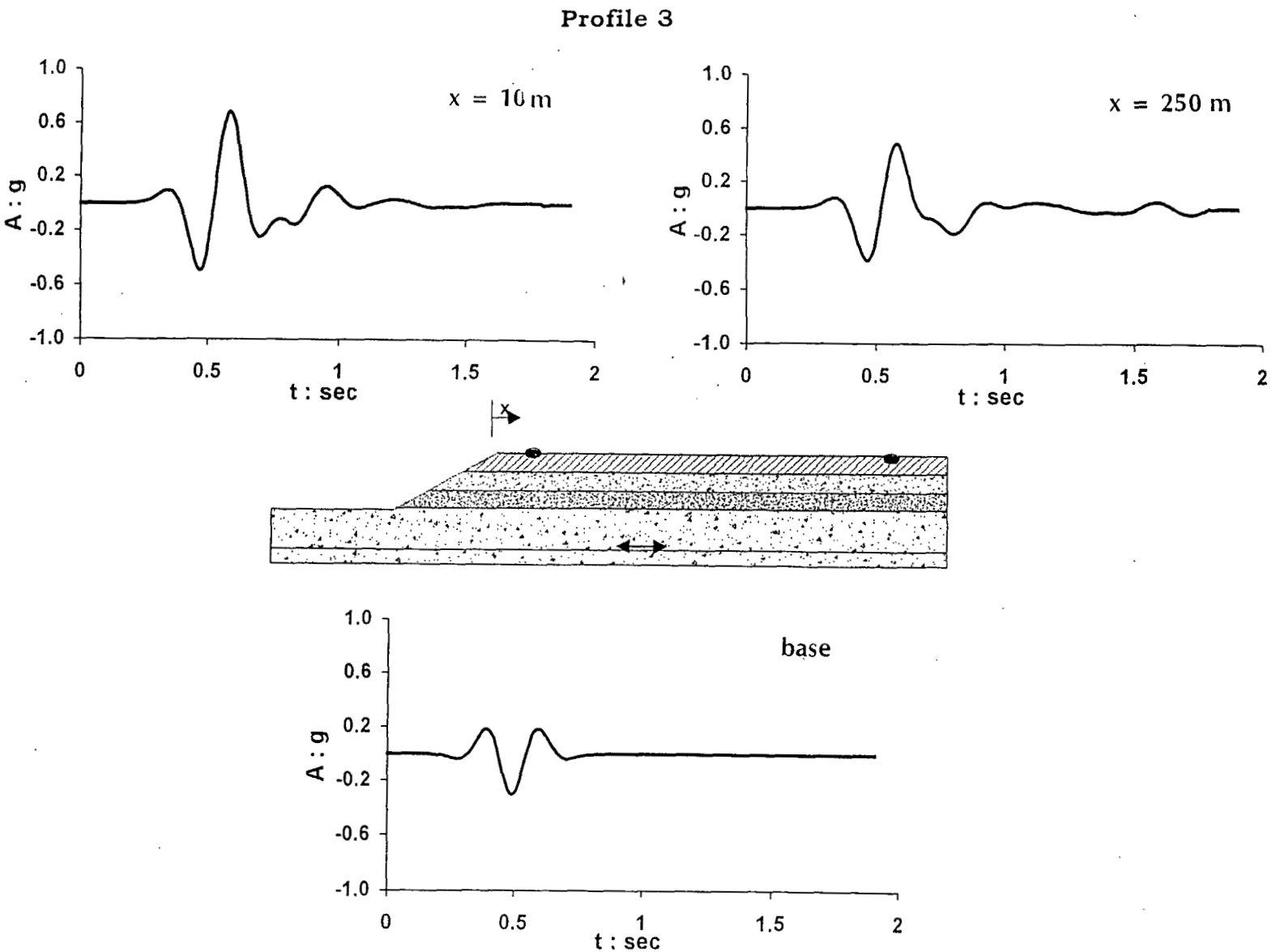

Figure 17

Adámes cliff with a layered halfspace (soil profile of Site 3): computed time histories of horizontal acceleration at x = 10 m (Site 3) and x = 250 m (Site 2). Ricker f_o = 3 Hz wavelet as vertical SV-wave excitation

Acceleration time histories of two surface points, at x = 10 m and x = 250 m from the crest, are compared with the *effective seismic input* motion (the base excitation) in **Figs. 15 - 17**. The three cases differ only in stiffnes and thicknes of the horizontal uniform soil layers : they correspond to the aforementioned profiles of Site 1, 2, and 3, respectively. We thus do not account *directly* for lateral soil heterogeneity -- a simplification of reality justified by the relatively small differences observed in the various soil profiles of Adámes. However, in the vertical direction, layering and inhomogeneity are modeled rigorously. In all three figures, both of the surface time-histories (the *synthetic accelerograms*, as one might call them) bear the consequences of *soil flexibility* (in the one-dimensional sense) : multiple reflections/transmissions of vertical S waves on/through the interfaces of the horizontal layers have led to amplification of motion. In addition however, the near-crest (x = 10 m) accelerogram has been further amplified by non-vertically propagating waves, arising from diffraction at the inclined boundary. Such 2-D waves decay rapidly away from crest and do not affect the motion at Site 2 (x = 250 m). This was confirmed through comparisons of the x = 250 m accelerogram with the one computed one-dimensionally for the particular profile and excitation. The three figures confirm our earlier finding that the soil profile of Site 2 gives rise to the strongest 1-D response (even if marginally). Moreover, the 2-D topographic amplification, measured through the ratio of peak values is as follows:

Profile	$maxA_{(x = 30\ m)}$ / $maxA_{(x = 250\ m)}$
1	0.79 / 0.61 ≈ 1.3
2	1.00 / 0.68 ≈ 1.5
3	0.69 / 0.49 ≈ 1.4

These ratios reveal *some* sensitivity to variations in the actual soil profile.

A more useful measure of topographic amplification in the frequency domain is defined as the ratio of the Fourier amplitude spectra at x = 10 m (≈ at the crest) and at x ≈ 250 m (in the free ground surface). Named ***Topographic Aggravation Factor,*** this ratio (denoted as AG) is plotted in **Fig. 18** as a function of frequency, f, for the three profiles. Evidently, AG reaches values of almost 2 and attains values in excess of about 1.5 in the frequency range f ≈ 3 – 6 Hz (roughly T ≈ 0.15 – 0.30 sec). These characteristics of the AG spectrum have been found to be equally stable with respect to the spectral content of the time function, using an f_o = 5 Hz Ricker and the six accelerograms describing the base motion.

The wave field affecting the surface motions consists of: (i) the vertically propagating incident SV wave; (ii) waves reflected at the horizontal ground surface and at the sloping surface of the cliff; (iii) waves transmitted through, and reflected at, layer interfaces, and (iv) *diffracted* waves. The latter include:

(a) SP waves that are generated at the cliff surface due to the critical on near-critical incidence of the vertical SV waves (the angle θ of the slope is $\theta \approx \theta_{cr} \approx \arcsin(V_S / V_P)$, for the realistic value of $\nu \approx 0.35$ of the Poisson's ratio of the sandy/clayey soils above the water table). Such waves propagate upward along the sloping surface.

(b) Rayleigh waves generated at the crest of the cliff.

The interference between these various types of direct and diffracted waves generates an increased motion near the crest and a rapidly varying motion (in amplitude and phase) along the horizontal ground surface.

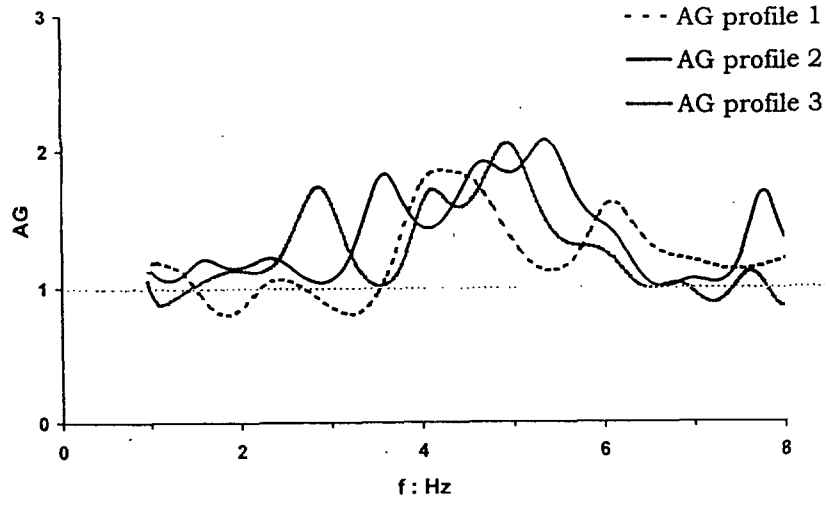

Figure 18

The spectrum of the *Topographic Aggravation Factor* (AG) computed with three soil profiles

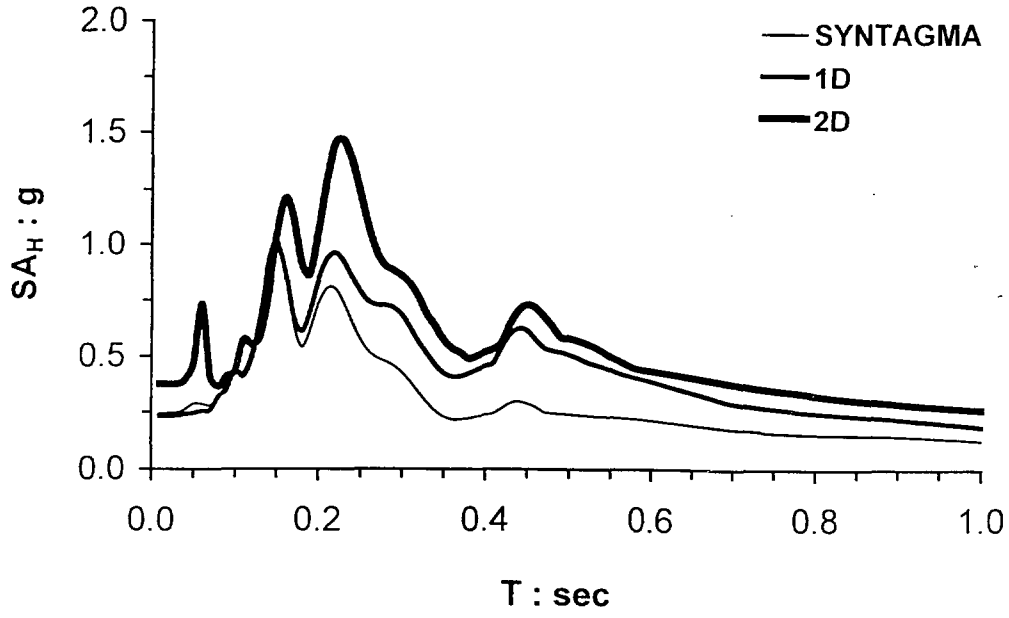

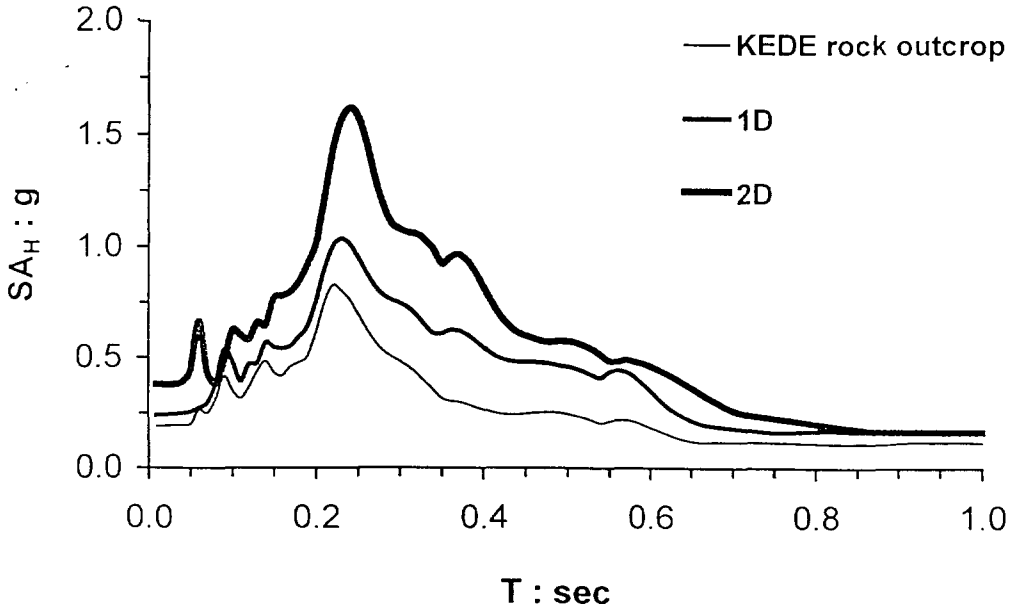

Figure 19(a) (is continued)

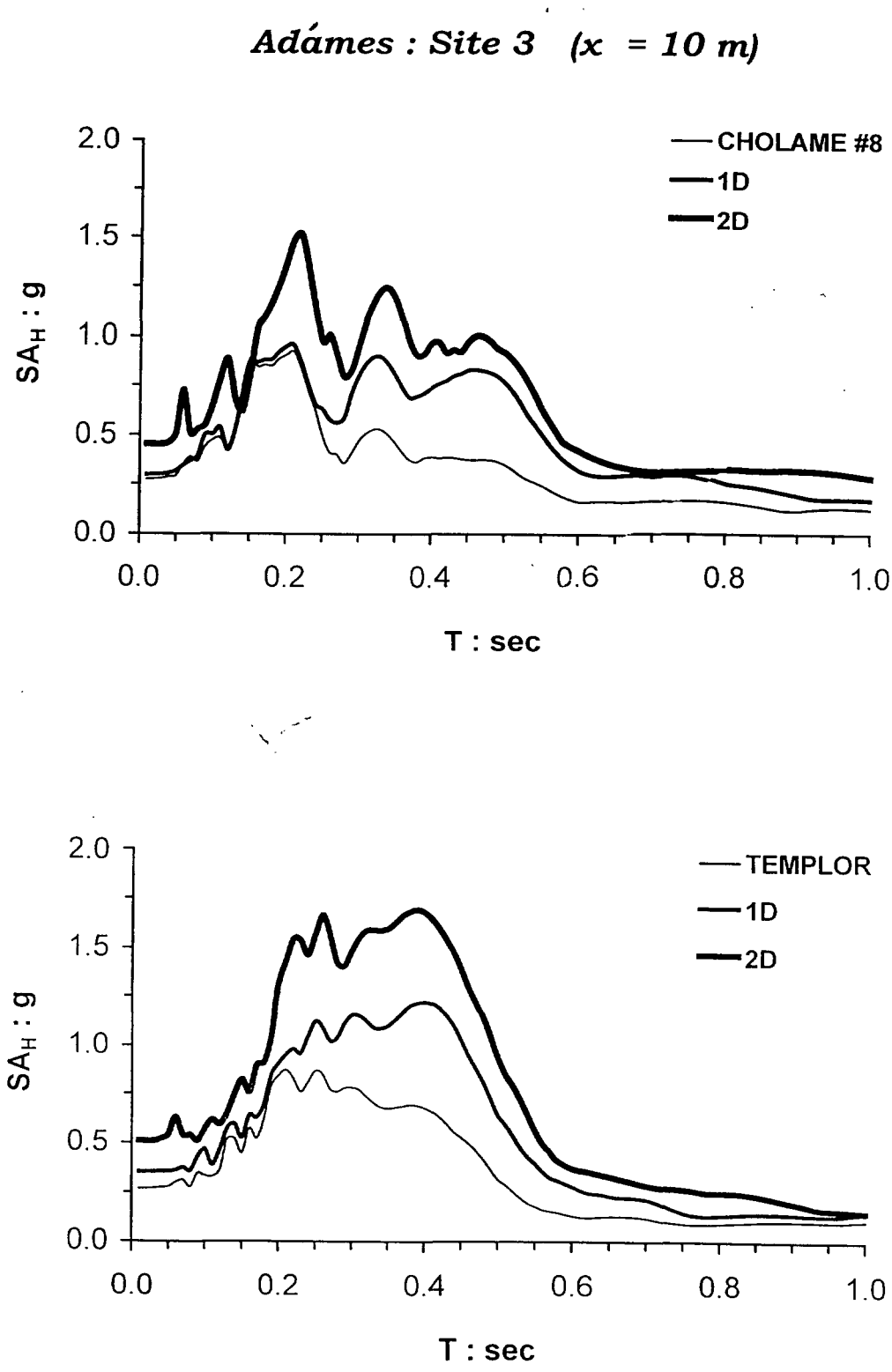

Figure 19(b) (continues)

Comparison of response spectra of: (i) rock-outcrop excitation, (ii) 1-D soil response analysis, and (iii) the complete 2-D analysis which accounts for both cliff topography and soil.

EXCITATION WITH STRONG-MOTION ACCELEROGRAMS --- CONCLUSION OF THE STUDY

Finally, the six candidate rock-outcrop accelererograms described in Section 3 are utilized to represent base excitation. Results are shown only for Site 3, for which the 2-D effects arising from the cliff have been shown to be significant. **Figs. 19 (a, b)** present the results in the form of acceleration response spectra for four of the aforementioned realistic excitations. The three spectra compared in each graph correspond to:

- the rock outcrop motion (excitation)
- the one-dimensionally computed motion which accounts only for the *soil flexibility* effect, and
- the two-dimensionally computed motion which accounts for both *soil flexibility* and *cliff topography*.

Apparently, the ratio of the 2-D to 1-D curves from each graph would offer a measure of the topographic amplification. In fact, as a crude approximation, this ratio could be taken as the aforementioned *Topographic Aggravation Factor*.

Then it becomes clear that, according to our computations, soil and topography have played an almost equal role in increasing the intensity of ground excitation. In the period range $T \approx 0.20$ to 0.60 seconds, where practically all the destroyed buildings (at least in Site 3) belonged to, the computed increase in spectral acceleration is by a factor of nearly 2.

Moreover, at least a visual comparison of the computed spectra with those of the original records in the center of Athens would be neccessary to correlate the results of analyses with damage observations in Adames. Indeed, such a comparison reveals that the motions computed for the Adámes' Site 3 are unquestionably the most devastating. For example, the KEDE record at $T \approx 0.30 - 0.40$ seconds has SA_H values of about 0.70 g – 0.30 g, respectively. The corresponding shaking in Adámes' Site 3 (subjected to KEDE-compatible excitation) has resulted in SA_H values of about 1.10 g – 0.80 g. (Note that the subscript H has been added in this concluding figure to emphasize the unquestionable presence during the earthquake of an accompanying vertical component of motion --- arising not only from direct P and non-vertical SV waves, as is always the case, but also from the waves diffracted from the cliff, as indicated in **Fig. 14**.)

Such comparisons would encourage one to attribute the observed damage concentration in Site 3 to combined soil and topographic effects. By contast, Site 2 appears to have been influenced only by 1-D soil amplification. However, our results are not as conclusive for Site 1, at least at this point in time, despite the undoubtedly negative role of soil flexibility.

Other potentially detrimental influences of 2-D wave-propagation, such as the enhancement of the collateral vertical component of motion; the increase in significant number of cycles of motion; the uncertain 2D role of the geologic structure at depths of the order of a few hundred meters; and the increase of 2-D "aggravation" when waves incide at an angle rather than vertically, have not been explored to sufficient depth to justify their reporting in this paper.

REFERENCES

Aki K. (1988): Local site effects on strong ground motion. Earthquake Engineering and Soil Dynamic II, ASCE.

Bard P. Y. (1982): Diffracted waves and displacement field over two dimensional elevated topographies, Geophys. J. R. Astr. Soc., 71, 731-760.

Bard P. Y. (1995). Effects of surface geology on ground motion: some results and remaining issues. 10th European Conference on Earthquake Engineering, Vienna, 1, 305-323.

Bard P. Y. & B. E. Tucker (1985): Ridge and tunnel effects: comparing observations with theory, BSSA, 75, 905-922.

Bielak, J. & P. Christiano (1984): On the effective seismic input for non-linear soil-structure interaction systems. Earthquake Engineering and Structural Dynamics 12: 107-119.

Boore D. M. (1972): A note on the effect of simple topography on seismic SH waves, BSSA, 62, 275-284.

Boucon M. & Barker J.S. (1996): Seiemic response of a hill: the example of Tarzana, CA . BSSA, 86, 66-72

Casadei F. & Gabellini E. (1997): Implementation of a 3D coupled spectral-element/finite-element solver for wave propagation and soil-structure interaction simulations. Technical Report, J. R. C., Ispra, Italy.

Celebi M. (1991): Topographical and geological amplification: Case studies and engineering applications. Structural Safety, 10, 199-217.

Delibasis N., Papadimitriou P., Voulgaris N., & Kassaras I. (2000): The Parnitha fault: A possible relationship with other neighboring faults and causes of larger damages. Annales Geologiques des pays Helleniques, 1e SERIE, T. XXXVIII, FASC. B, 41-50.

Dobry R. et al (2000): New site coefficient and site classification system used in recent building seismic code provisions. Earthquake Spectra, 16, 41-67.

Faccioli E., Maggio F., Paolucci R., Quarteroni A. (1997): 2-D and 3-D elastic wave propagation by a pseudo-spectral domain decomposition method. Journal of Seismology 1: 237-251.

Faccioli E., Paolucci R., & Vanini M., editors (1998): TRISEE: 3D site effects and soil-foundation interaction in earthquake and vibration risk evaluation. EC.

Faccioli E. (1991): Seismic amplification in the presence of geologic and topographic irregularities. 2nd Int. Conf. on Recent advances in Geotechnical Earthquake Engineering, St. Louis, II, 1779-1797.

Finn W.D.L. (1991): Geotechnical Engineering aspects of Microzonation. Int. Microzonation Conference, Stanford, 1, 199-259.

Hibbit, Karlsson, & Sorensen Inc. (1997): ABAQUS.

Gazetas G., Dakoulas P., & Papageorgiou A. S. (1990): Local soil and source mechanism effects in the 1986 Kalamata (Greece) earthquake. Earthq. Engrg. & Struct. Dyn., 19, 431-456.

Geli L., P. Y. Bard, & B. Jullien (1988): The effect of topography on earthquake ground motion: A review and new results. BSSA, 78, 42-63.

Kawase H. & K. Aki 1990: Topography effect at the critical SV-wave incidence: possible explanation of damage pattern by the Whittier Narrows, California, earthquake of 1 October 1987. BSSA, Vol. 80, pp. 1-22

Leeds D. J. (1992): Recommended accelerograms for earthquake ground motions. USAE Waterways Experiment Station. Report 28, S-73-1.

Loukakis K. (1988): Transient response of shallow layered valleys for inclined SV waves calculated by the finite-element method. MS Thesis. Carnegie Mellon University.

Ohtsuki A. and Harumi K. (1983): Effect of topography and subsurface inhomogeneities on seismic SV waves. Earthq. Engrg. & Struct. Dyn., 11, 441-462.

Paolucci R., Faccioli E., & Maggio F. (1999): 3D response analysis of an instrumented hill at Matsuzaki, Japan, by a spectral method. Jnl of Seismology, 3, 191-209

Papadimitriou P., Voulgaris N., Kassaras I., Delibasis N., & Makropoulos K. (2000): The September 7, 1999 Athens earthquake sequence recorded by the Cornet network: preliminary results of source parameter determination of the mainshock. Annales Geologiques des pays Helleniques, 1e SERIE, T. XXXVIII, FASC. B, 29-40.

Papadopoulos G. A., Drakatos G., Papanastasiou D., Kalogeras I., & Stavrakakis G. (2000): Preliminary results about the catastrophic earthquake of 7-9-99 in Athens. Seismological Research Letters, 71, 318-329.

Restrepo J. I. & Cowan H. A. (2000): The "Eje Cafetero" earthquake, Colombia of January 25 1999. Bull. New Zea. Soc. of Earthq. Engrg, 33, 1-29
Sanchez-Sesma & Campillo (1991)

Rondogianni Th., Mettos A., Galanakis D., & Georgiou Ch. (2000): The Athens earthquake of September 7, 1999: its setting and effects. Annales Geologiques des pays Helleniques, 1e SERIE, T. XXXVIII, FASC. B, 131-144.

Sanchez-Sesma F. J. (1985): Diffraction of elastic SH waves by wedges. BSSA, 75, 1435-1446.

Sanchez-Sesma et al (1999): Fundamentals of elastic wave propagation for site amplification studies. UNAM Report, Mexico.

Shakal A., Huang M., & Cao T. (1988): The Whittier Narrows California earthq. of October 1, 1987: CSMIP strong motion data. Earthquake Spectra, 4, 75-100

Schnabel P. B., Lysmer J., & Seed H. B. (1972): SHAKE. Report EERC 72-12 UC Berkeley.

Siro L. (1982): Emergency microzonations by Italian Geodynamics Project, after November 23, 1980 earthq. 3rd Int. Conf. on Microzonation, Seattle, 3, 1417-1427.

Stavrakakis G. (1999): Athens Earthquake of September 7, 1999. News Letter of the European Centre on Prevention and Forecasting of Earthquakes, No. 3, 26-29.

Voulgaris N., Kassaras I., Papadimitriou P, & Delibasis N. (2000): Preliminary results of the Athens aftershock sequence. Annales Geologiques des pays Helleniques, 1e SERIE, T. XXXVIII, FASC. B, 51-62.

Vucetic M. & Dobry R. (1991): Effect of soil plasticity on cyclic response. Journal of Geotechnical Engineering, ASCE 117: 89-107.

Wong H. L. & Trifunac M. D. (1974): Scattering of plane SH waves by semi-elliptical canyon. Earthq. Engrg. & Struct. Dyn., 3, 157-169.

Wong H.L. & Jennings P.C. (1975): Effect of canyon topography on strong ground motion. BSSA, 72, 1167-1183.

Yegian M. K., Ghachraman V. G., & Gazetas G. (1994): Seismological, soil, and valley effects in Kirovakan, 1988 Armenia earthquake. Journal of Geotechnical Engineering, ASCE, 120, 349-365.